Rare Met. (2024) 43(5):2172–2183
https://doi.org/10.1007/s12598-024-02675-z

RARE METALS

ORIGINAL ARTICLE

Regulated polarization degree of upconversion luminescence and multiple anti-counterfeit applications

Dong-Ping Wen, Ping Chen*, Yi Liang, Xiao-Ming Mo, Cao-Feng Pan*

Received: 8 May 2023 / Revised: 12 July 2023 / Accepted: 13 July 2023 / Published online: 25 March 2024

Abstract Polarization upconversion luminescence (PUCL) of lanthanide ions (Ln^{3+}) has been widely used in single particle tracking, microfluidics detection, three-dimensional displays, and so on. However, no effective strategy has been developed for modulating PUCL. Here, we report a strategy to regulate PUCL in Ho^{3+}-doped $NaYF_4$ single nanorods based on the number of upconversion photons. By constructing a multiphoton upconversion system for Ho^{3+}, we regulate the degree of polarization (DOP) of PUCL from 0.590 for two-photon luminescence to 0.929 for three-photon upconversion luminescence (UCL). Furthermore, our strategy is verified from cross-relaxation between Ho^{3+} and Yb^{3+}, excitation wavelength, excitation power density, and local site symmetry. And this regulation strategy of PUCL has also been achieved in Tm^{3+}, with the DOP ranging from 0.233 for two-photon luminescence to 0.925 for four-photon UCL. Besides, multi-dimensional anti-counterfeiting display has been explored with PUCL. This work provides an effective strategy for regulating PUCL and also provides more opportunities for the development of polarization display, optical encoding, anti-counterfeiting, and integrated optical devices.

Keywords Polarization upconversion luminescence; Degree of polarization; Population density of excited state; Number of upconversion photons; Polarization anti-counterfeiting display

1 Introduction

Polarization upconversion luminescence (PUCL) of lanthanide ions (Ln^{3+}) is the anisotropic emission induced by the local site symmetry around Ln^{3+} [1–3]. PUCL has developed applications in optical storage, biological imaging [4–9], polarization displays, biotracking and microfluidic probes [10–14]. The adjustable polarized luminescence from Ln^{3+} can provide a strong guarantee for biological probes and three-dimensional display [15–21]. In particular, highly polarized luminescence has great potential applications in multiple anti-counterfeiting encryption and display [22–29]. However, due to the diversity of Ln^{3+} and the complexity of the electronic structure of trivalent 4f ions [30, 31], there is no effective control strategy for controlling the PUCL. The polarized luminescence of Ln^{3+} is influenced not only by the local site symmetry of the crystal field (CF) but also many other factors, such as the direction of electric field of the excitation field, the energy transfer between Ln^{3+}, the concentration of activators, and plasmonic nanomaterials with a specific structure [32–37]. In order to control the polarized luminescence of Ln^{3+} from a single nanorod, attempts

Dong-Ping Wen and Ping Chen have contributed equally to this work.

Supplementary Information The online version contains supplementary material available at https://doi.org/10.1007/s12598-024-02675-z.

D.-P. Wen, P. Chen*, Y. Liang, X.-M. Mo, C.-F. Pan
Center On Nanoenergy Research, Guangxi Key Laboratory for Relativistic Astrophysics, School of Physical Science and Technology, Guangxi University, Nanning 530004, China
e-mail: chenping@gxu.edu.cn

C.-F. Pan*
Key Laboratory of Micronano Energy and Sensor, CAS Center for Excellence in Nanoscience, Beijing Institute of Nanoenergy and Nanosystems, Chinese Academy of Sciences, Beijing 100140, China
e-mail: cfpan@binn.cas.cn

have been made to vary the concentration of sensitizers and activators [32, 33]. However, it is still difficult to tune PUCL and achieve highly polarized luminescence from Ln^{3+}.

Site symmetry around Ln^{3+} is essential for PUCL [1–3]. In the hexagonal phase of $NaYF_4$, point group symmetry is C_s and energy states of Ln^{3+} are represented by different irreducible Γ_n [38]. Electrons are pumped from ground state (GS) to excited state (ES) $^{2s+1}L_J$, where the states are split into different Stark energy levels and presented as irreducible representations (Γ_n). The ES undergoes a non-radiative (NR) or radiative transition and decays to the GS. This essential process for radiative transition is irreducible transition from Γ_n (ES) $\rightarrow$ Γ_m (GS) ($m \neq n$) [39]. Some transition dipoles, such as s and p configurations, exhibit excitation polarization dependence or emission anisotropy [3, 40]. The polarization of the upconversion luminescence (UCL) originates from the mixture of different dipole transitions Γ_n (ES) $\rightarrow$ Γ_m (GS). Therefore, constructing an energy system for multiphoton upconversion can broaden the distribution of irreducible transitions $\Gamma_n \rightarrow \Gamma_m$ with various mixture states at multiple ESs. Here, we choose Ho^{3+} and Tm^{3+} as activators due to that they possess rich ladder-type energy levels and multi-color emissions, corresponding to multiple photon upconversion processes [41, 42]. This brings more possibilities for our regulation of excitation polarization luminescence and extending the application to multiple anti-counterfeiting displays. Despite the promising performance of Ho^{3+} and Tm^{3+}, the regulation of PUCL by the NR transitions therein remains a challenge.

In this work, we report a strategy to modulate the PUCL based on the multiphoton upconversion processes. The polarization of multiple emissions is regulated by the number of photons in the multiphoton upconversion process constructed in Ho^{3+}, where the degree of polarization (DOP) of three-photon process is larger than that of two-photon process. With the exclusion of the CF, our mechanistic studies show that the multiphoton upconversion process can be pumped to a higher ES, which is less affected by NR transitions. The population density of higher ESs is lower, and the mixture of electron configuration for irreducible transitions Γ_n (ES) $\rightarrow$ Γ_m (GS) is fewer. That is, dipole orientations for irreducible transitions in higher ESs are not too much complicated. Thus, the proportion of dipole transitions in a similar direction is larger, resulting in a larger DOP of PUCL. The DOP exhibits an inverse relationship with the population density of ESs, which determines the strength of mixed irreducible transitions Γ_n (ES) $\rightarrow$ Γ_m (GS) and mixed dipole orientations. Therefore, we can tune the DOP of PUCL by controlling the number of photons in upconversion process. This regulatory strategy has been verified not only in Ho^{3+} but also in Tm^{3+}. The DOP is regulated from 0.925 for four-photon process to 0.233 for two-photon process in $NaYF_4$: Yb, Tm single nanorods. This highly polarized and tunable UCL is applied in multi-dimensional anti-counterfeiting displays.

2 Results and discussion

2.1 Constructed multiphoton upconversion energy system for regulating PUCL

In our work, we need to construct an energy system for multiphoton upconversion transitions to generate PUCL and realize polarization regulation. In the traditional multiphoton upconversion process by excited state absorption (ESA), ground state absorption (GSA) occurs once energy resonance of pump photon with the energy from the GS to the first ES_1 of Ln^{3+}. As a result, metastable state ES_1 is pumped, followed by absorbing another pumped photon by ESA to generate ES_2. Then, ES_2 undergoes a radiative transition, producing two-photon UCL Em_1 (Fig. 1) [43]. Analogously, ES_3 gives rise to three-photon UCL, Em_2 and so on. According to:

$$N_2 \propto N_1^2 \,(\text{i.e.}, N_1 < 1) \tag{1}$$

where N_1 and N_2 are the population density of the ES_1 and ES_2, respectively [44]. More energy state $|i\rangle$ are analogized. The energy state of ES_4 pumped by the four-photon upconversion process is greater than that of two-photon process, resulting in a lower population density ($N_4 < N_2$). Thus, under the same excitation power, the population density of ESs with four-photon process is much smaller than that of two-photon process. Therefore, we can control the population density of ES_i by the number of photons in upconversion process.

In the hexagonal phase of $NaYF_4$, the $^{2s+1}L_J$ energy level of Ln^{3+} can split into the $2J + 1$ energy levels corresponding to irreducible Γ_n symmetry [39, 40], due to the C_s point group symmetry [38]. The irreducible transitions Γ_d (ES_3) $\rightarrow$ Γ_a (GS) ($d \neq a$) generate UCL for the three-photon upconversion process (Fig. 1). Among these transitions, some transition dipoles exhibit excitation polarization dependence for dipole orientation. But the dipole orientations might vary from each other, such as s and p polarization. And the lots of mixed dipole orientations reduce the probability of similar dipole orientations and result in low or canceled PUCL. Thus, the DOP of PUCL depends on mixed irreducible transitions Γ_d (ES_3) $\rightarrow$ Γ_a (GS) with different dipole orientations. Compared with the three-photon upconversion process, the population density of the ES_4 is lower due to four-photon upconversion process and the low energy transfer

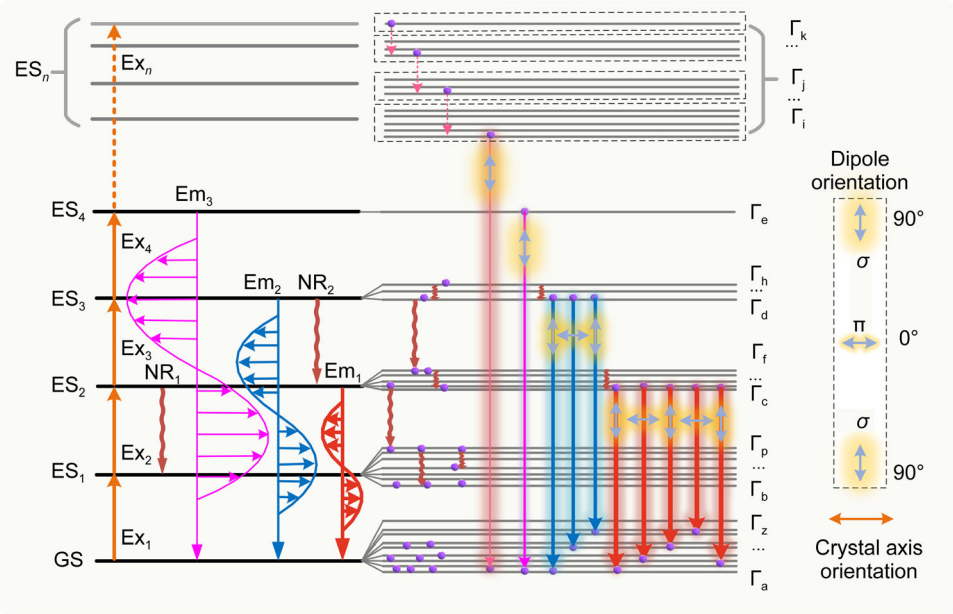

Fig. 1 Schematic diagram of multiphoton enhancement of DOP of PUCL in Ln^{3+}

efficiency. And the mixing of different dipole orientations is reduced, leading to a similar orientation and a higher DOP for PUCL. In contrast, the population density of the ES_2 is larger for two-photon upconversion process due to the less photons for UCL. As a result, the possibility of mixed different orientations of dipole transitions increases, and DOP of PUCL is smaller or even disappeared. Therefore, the number of upconversion photons influences the population density of ESs and DOP of PUCL through the irreducible transition Γ_i (ES_n) → Γ_a (GS) with different dipole orientations (Fig. 1). However, the number of upconversion photons and the population density of ES_i are also affected by NR transitions such as energy transfer, cross-relaxation, and excitation wavelength in the traditional upconversion process. We expect to control the DOP of PUCL through tuning the population density of ES_i by the number of upconversion photons, accompanying with the interaction of NR transitions and the excitation wavelength.

2.2 Highly polarized $NaYF_4$: Ho upconversion luminescence nanorods

Ho^{3+} is chosen first to realize the modulation of DOP by the number of upconversion photons for its excellent photochemical stability and ladder-type energy levels. $NaYF_4$: Ho nanorods (length ~ 1460 ± 200 nm, diameter ~ 108 ± 20 nm) are synthesized by a typical hydrothermal method (Fig. S1a, b), and all nanorods exhibit excellent uniformity in length and elemental distribution (Figs. S1c, S2b). Optical measurements of single nanorod are realized by home-built micro-region platform (Fig. 2a), where a half-wave plate is placed in the excitation path to change the direction of the electronic field of excitation light. Under the excitation of an 1150 nm laser, the UCL spectra (Fig. 2c) from $NaYF_4$: Ho single nanorod are obtained. Four emission peaks are presented, centered around 486, 541, 750 and 648 nm, respectively, corresponding to the four transitions of Ho^{3+}: $^5F_3 \rightarrow {}^5I_8$, $^5F_4/^5S_2 \rightarrow {}^5I_8$, $^5F_4/^5S_2 \rightarrow {}^5I_7$ and $^5F_5 \rightarrow {}^5I_8$, respectively. Then, PUCL spectra of $NaYF_4$: Ho single nanorod can be obtained (Fig. 2c) by changing the polarization direction of the excitation laser (Fig. 2a). Anisotropic absorption is first excluded due to the vertical relationship between the orientation of polarized luminescence and anisotropic absorption (Figs. S1d, S2a, b). The luminescence intensities of the four transitions show the same trend with varying polarization angles. All of the transitions appear a period of 180° by fitting the luminescence intensities using:

$$y = y_0 + A \cdot \sin^2(\theta) \quad (2)$$

function (Fig. S1d), where y_0 and A are constants, and θ is polarization angles. The DOP is defined as:

$$\mathrm{DOP} = (I_{\max} - I_{\min})/(I_{\max} + I_{\min}), \quad (3)$$

where $I_{\max}$ and $I_{\min}$ are the maximum and minimum intensities of integrated UCL, respectively. The DOPs for the $^5F_3 \rightarrow {}^5I_8$, $^5F_4/^5S_2 \rightarrow {}^5I_8$, $^5F_4/^5S_2 \rightarrow {}^5I_7$ and $^5F_5 \rightarrow {}^5I_8$ transitions are calculated to be 0.833, 0.828, 0.824 and 0.651, respectively. It is interesting that the DOPs of $^5F_3 \rightarrow {}^5I_8$, $^5F_4/^5S_2 \rightarrow {}^5I_8$, and $^5F_4/^5S_2 \rightarrow {}^5I_7$ transitions are close to each other and larger than the DOP from the

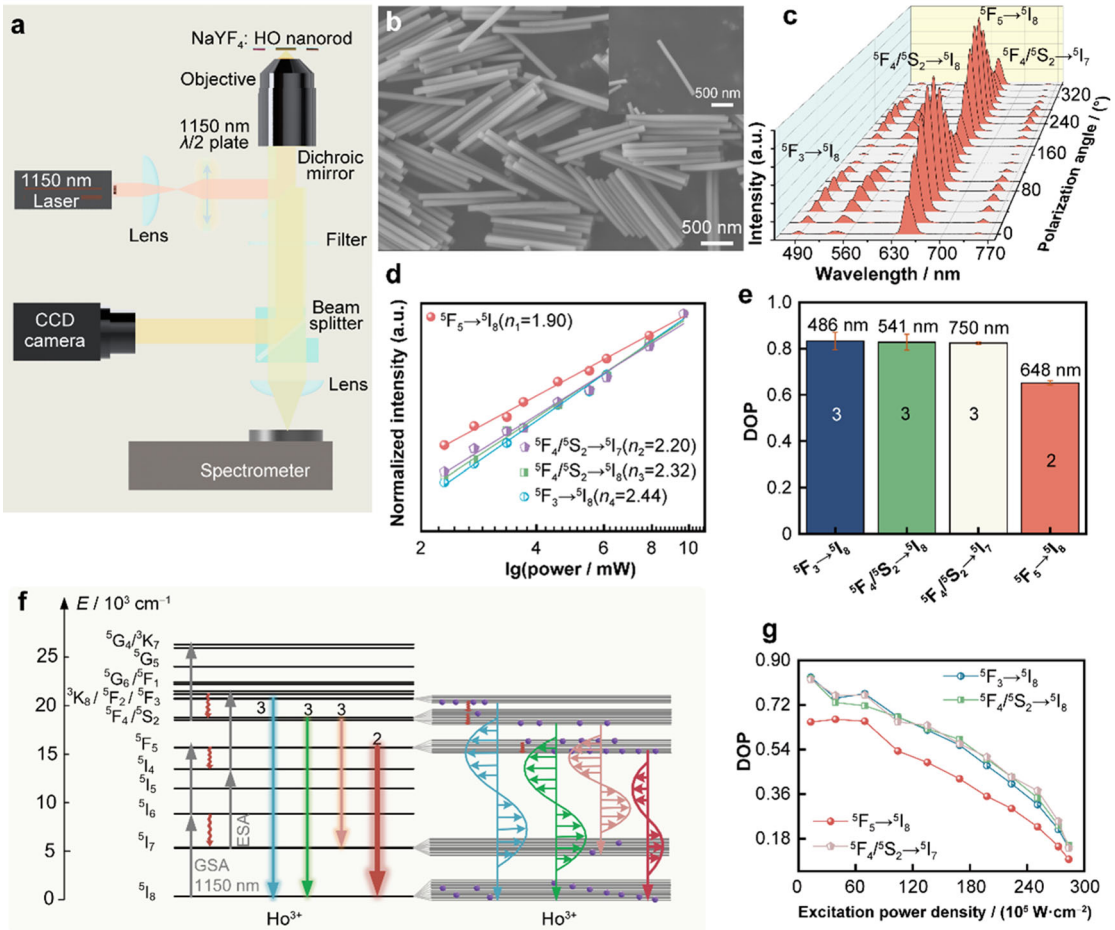

Fig. 2 Regulated DOP of PUCL from Ho^{3+} based on number of upconversion photons: **a** schematic illuminated UCL of $NaYF_4$: 8%Ho single nanorods collected by a home-built optical micro-region system; **b** SEM image of $NaYF_4$:8%Ho nanorods and (inset) single nanorod; **c** PUCL spectra of $NaYF_4$: 8%Ho single nanorod excited at 1150 nm, where excitation power at 1150 nm for all tests was 11.8 mW at ×100 objective, unless otherwise stated; **d** upconversion emission intensity as a function of excitation power for $NaYF_4$: 8%Ho single nanorod excited by 1150 nm; **e** histogram illustrating photon number connected DOPs of four transitions; **f** schematic diagram of multiphoton upconversion mechanism of Ho^{3+} excited at 1150 nm, accompanying with population density of ES_i and DOPs of different transitions; **g** dependence of DOP on pump power density of excitation light

transition of $^5F_5 \rightarrow {}^5I_8$. According to the relationship between the DOP and the number of upconversion photons, this phenomenon implies that the number of upconversion photons for $^5F_3 \rightarrow {}^5I_8$, $^5F_4/{}^5S_2 \rightarrow {}^5I_8$, and $^5F_4/{}^5S_2 \rightarrow {}^5I_7$ transitions is consistent and larger than the number of photons for the $^5F_5 \rightarrow {}^5I_8$ transition.

Excitation power dependence of single nanorod is carried out to assess the upconversion process (Fig. 2d). The number of photons (n) required to populate the emitting state can be calculated by the relation of:

$$I_{em} \propto P^n \tag{4}$$

where I_{em} is the integral intensity of UCL, and P is the pump power of the laser [44]. The value of n_1 is 1.90, which corresponds to the $^5F_5 \rightarrow {}^5I_8$ transition, indicating that two photons are required to pump the $^5F_5$ state. The value of n_2, n_3 and n_4 for the three transitions of $^5F_4/{}^5S_2 \rightarrow {}^5I_7$, $^5F_4/{}^5S_2 \rightarrow {}^5I_8$ and $^5F_3 \rightarrow {}^5I_8$ is 2.20, 2.32 and 2.44, respectively, suggesting the three-photon upconversion process. Thus, the DOPs of the transitions with three-photon pumping are larger than that of the transition with a two-photon process (Fig. 2e). This verifies our strategy to regulate the polarized luminescence based on the number of upconversion photons. The more the number of photons which are needed in upconversion process, the less the population density of ESs which are presented and the larger DOP of PUCL it becomes.

The DOPs of different transitions are regulated by the population density of ES_i. In the typical multiphoton upconversion transition process of Ho^{3+} excited at 1150 nm (Fig. 2f), $^5F_3 \rightarrow {}^5I_8$, $^5F_4/{}^5S_2 \rightarrow {}^5I_8$, $^5F_4/{}^5S_2 \rightarrow {}^5I_7$ are three-photon upconversion processes and $^5F_5 \rightarrow {}^5I_8$ is a two-photon upconversion process, where the ESs of $^5F_4/{}^5S_2$ originate from the NR transition of the $^5F_3$

state. Any transition is a mixture of irreducible transitions Γ_n (ES) → Γ_m (GS) with various dipole orientations [45]. Compared with the three-photon process, the two-photon process has a larger population density of ES. Thus, the mixing probability of different dipole orientations from two-photon process is much larger than those of the three-photon processes, resulting in a lower DOP. These phenomena are consistent with our proposed regulation strategy, indicating that the DOP of PUCL can be adjusted by modulating the population density of ESs.

Furthermore, the population density of ESs can be controlled by the pump power of the excited source, and thus, the DOP of PUCL can be operated by the pump power density of the excitation light. Since the relationship:

$$N_i \propto P^n \tag{5}$$

where N_i is the population density of ESs and P is the excitation power [46], the population density of ESs (N_i) will increase with enhancing excitation power (P). Here, the statistics of DOP from a single nanorod on excited power are presented (Fig. 2g). It is found that the DOPs decrease for all of the upconversion transitions as the excitation power increases. But the DOPs from three-photon transitions are still kept higher than that from two-photon transition at any power. Moreover, the DOPs are reduced to close to 0 for all the transitions, and PUCL is almost disappeared accompanying with much enhanced UCL intensity when the power is large enough. This is due to that the ESs of four transitions approach saturation at high power [46], inducing strong mixing of different dipole orientations from irreducible transitions Γ_m (ES) → Γ_n (GS) for any emission bands. Hence, the UCL is depolarized. The diminished trend of DOPs with increasing power indicates that the saturated population of ESs suppresses the PUCL from Ln^{3+}. Furthermore, the population density of ESs can dominate the DOP, which verifies the polarized strategy regulated by the number of upconversion photons.

2.3 Cross-relaxation and the number of upconversion photons tune DOPs of PUCL

The number of upconversion photons and the population density of ESs are also affected by NR transitions such as cross-relaxation. The DOP strategy based on the number of upconversion photons is still effective with cross-relaxation. Here, we introduced cross-relaxation between Yb^{3+} and Ho^{3+} to monitor the DOPs from Ho^{3+} (Fig. S3) [42]. The same emission peaks are detected under 1150 nm excitation (Fig. S4a), and PUCL also exhibits a periodic change of 180° with changing the polarization angle of the excitation light (Figs. 3a, S4b). The DOPs are 0.623 and 0.590 for the two-photon transitions $^5F_4/^5S_2 \rightarrow {}^5I_8$ and $^5F_4/^5S_2 \rightarrow {}^5I_7$, respectively (Fig. 3b, c). Both of the transitions come from the same ESs of $^5F_4/^5S_2$ and present similar DOPs. Meanwhile, the DOPs are 0.800 and 0.929 for the three-photon transitions $^5F_5 \rightarrow {}^5I_8$ and $^5F_3 \rightarrow {}^5I_8$, respectively (Fig. 3b, c). Obviously, the DOPs of two-photon transitions are significantly smaller than those of three-photon transitions, which is consistent with the polarization strategy regulated by the number of upconversion photons. It is interesting that the $^5F_4/^5S_2 \rightarrow {}^5I_8$ and $^5F_4/^5S_2 \rightarrow {}^5I_7$ transitions are two-photon processes in $NaYF_4$: Yb, Ho single nanorod, while those are three-photon processes in $NaYF_4$: Ho single nanorod, indicating different pump paths for the same transitions. The anomalous upconversion pathways of the $^5F_4/^5S_2 \rightarrow {}^5I_8$, $^5F_4/^5S_2 \rightarrow {}^5I_7$, and $^5F_5 \rightarrow {}^5I_8$ transitions in nanorods are caused by cross-relaxation between Yb^{3+} and Ho^{3+} when excited by 1150 nm (Figs. 3d, S4c, d). These results indicate that the DOPs of PUCL are determined by the population density of ESs in the energy levels.

2.4 Excitation wavelength regulates DOPs of PUCL

The number of upconversion photons is correlated with the wavelength of excitation light. Generally speaking, for the same ES, the number of required upconversion photons with high energy is less than that with low energy because of the different pumping path. We changed the excitation wavelength to 975 nm to vary the pump path and regulate DOP (Figs. 4a, S5a, b). DOPs for two-photon transitions $^5F_4/^5S_2 \rightarrow {}^5I_8$ and $^5F_4/^5S_2 \rightarrow {}^5I_7$ are 0.166 and 0.155, respectively. And DOPs for three-photon process $^5F_5 \rightarrow {}^5I_8$ and $^5F_3 \rightarrow {}^5I_8$ transitions are 0.221 and 0.273, respectively (Fig. 4b, c). The greater the number of photons required, the higher the DOPs of UCL, which is consistent with our proposed strategy of controlling the DOP by the number of photons. In addition, DOP of $^5F_5 \rightarrow {}^5I_8$ transition is smaller than that of $^5F_3 \rightarrow {}^5I_8$ transition, although the same number of photons is required for both transitions. The difference is originated from the various pump channels. The $^5F_5$ state comes from two paths. One way is the general two-photon upconversion process. The other way is the three-photon process with cross-relaxation (CR1): $^5G_4/^3K_7$ (Ho^{3+}) + $^2F_{7/2}$ (Yb^{3+}) → $^5F_5$ (Ho^{3+}) + $^2F_{5/2}$ (Yb^{3+}) (Fig. S5c). While $^5F_3$ state is pumped by three-photon absolutely. Thus, the population density of $^5F_5$ state is higher than that of $^5F_3$ state, resulting in a lower DOP for the $^5F_5 \rightarrow {}^5I_8$ transition.

The population density of ESs is also tuned by the synergistic effect of excitation wavelength and Yb^{3+} doping based on the number of upconversion photons. When excited by 975 nm, the population density of ESs will have a significant increment because of the larger absorption

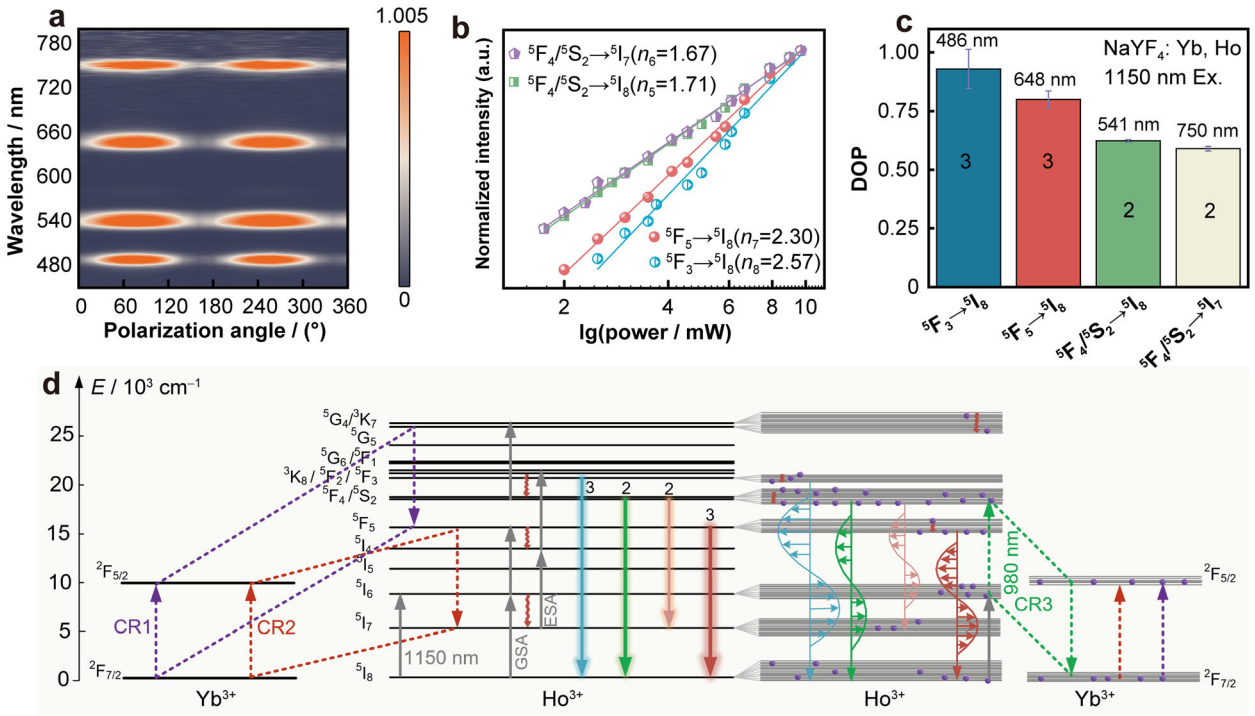

Fig. 3 Tunable DOPs of PUCL from Ho^{3+} with cross-relaxation modulated number of upconversion photons: **a** matrix diagram of PUCL from $NaYF_4$: 20%Yb, 8%Ho single nanorod excited by 1150 nm; **b** upconversion emission intensity as a function of excitation power for $NaYF_4$: 20%Yb, 8%Ho single nanorod excited by 1150 nm; **c** histogram illustrating photon number connecting DOPs of four transitions; **d** schematic illustration of multiphoton upconversion mechanism of $NaYF_4$: Yb, Ho excited at 1150 nm, accompanying with population density of ES_i and DOPs of different transitions

cross of Yb^{3+} and more efficient energy transfer from Yb^{3+} to Ho^{3+} [47–49]. The higher population density of ESs can induce a strong mixing of different dipole orientations and lead to a low DOP. Indeed, with the same number of upconversion photons, the DOPs are 0.221 and 0.273 for $^5F_5 \rightarrow {}^5I_8$ and $^5F_3 \rightarrow {}^5I_8$ transitions (Fig. 4c), respectively, in Yb^{3+} co-doped single nanorod with 975 nm excitation, while they are 0.800 and 0.929 in the same single nanorod with 1150 nm excitation (Fig. 3c). The same situation exists for two-photon $^5F_4/^5S_2 \rightarrow {}^5I_8$ and $^5F_4/^5S_2 \rightarrow {}^5I_7$ transitions (Figs. 3c, 4c). The remarkable reduction of DOPs from Yb^{3+} co-doped single nanorod reconfirms the regulated strategy of population density of ESs and the number of upconversion photons.

The regulated strategy based on the number of upconversion photons keeps working with the changing local site symmetry around activators. It has been reported that the bonding length and bonding angles between Ln^{3+} and F^- are altered with co-doped Gd^{3+} into nanorods, which changes the local symmetry and polarized behavior of Ln^{3+} [1, 50]. In this section, we introduced a high concentration of Gd^{3+} into Ho^{3+}-doped nanorods (Figs. 4d, S6a). The DOPs for $^5F_3 \rightarrow {}^5I_8$, $^5F_4/^5S_2 \rightarrow {}^5I_8$ and $^5F_4/^5S_2 \rightarrow {}^5I_7$ transitions are 0.867, 0.878 and 0.814 (Fig. S6c), which are three-photon upconversion processes (Fig. S6b). And the DOP for $^5F_5 \rightarrow {}^5I_8$ transition is 0.686 (Fig. S6c), which is a two-photon upconversion process (Fig. S6b). Notably, the DOPs of three-photon upconversion are higher than that of the two-photon process. Thus, the presented performance is in line with regulated strategy.

2.5 Tunable DOPs of PUCL from Tm^{3+} based on number of upconversion photons

The regulated strategy of DOPs based on the number of upconversion photons can be extended to Tm^{3+} due to the excellent ladder-type energy levels to realize multiphoton upconversion [41]. The UCL spectra from $NaYF_4$: Yb, Tm single nanorod (Fig. 5a) present five emission bands upon excitation at 975 nm (Fig. 5b). The emission bands are centered around 452, 476, 648, 695 and 792 nm, corresponding to $^1D_2 \rightarrow {}^3F_4$, $^1G_4 \rightarrow {}^3H_6$, $^1G_4 \rightarrow {}^3F_4$, $^3F_3 \rightarrow {}^3H_6$ and $^3H_4 \rightarrow {}^3H_6$ transitions of Tm^{3+}, respectively. Then, the luminescence intensity was normalized by the deconvolution method and fitted by the function Eq. (2) (Fig. 5c). It is found that three kinds of DOPs are presented, corresponding to different upconversion modes. First is the two-photon upconversion path (Fig. 5d); the DOPs of $^3F_3 \rightarrow {}^3H_6$ and $^3H_4 \rightarrow {}^3H_6$ transitions are 0.233

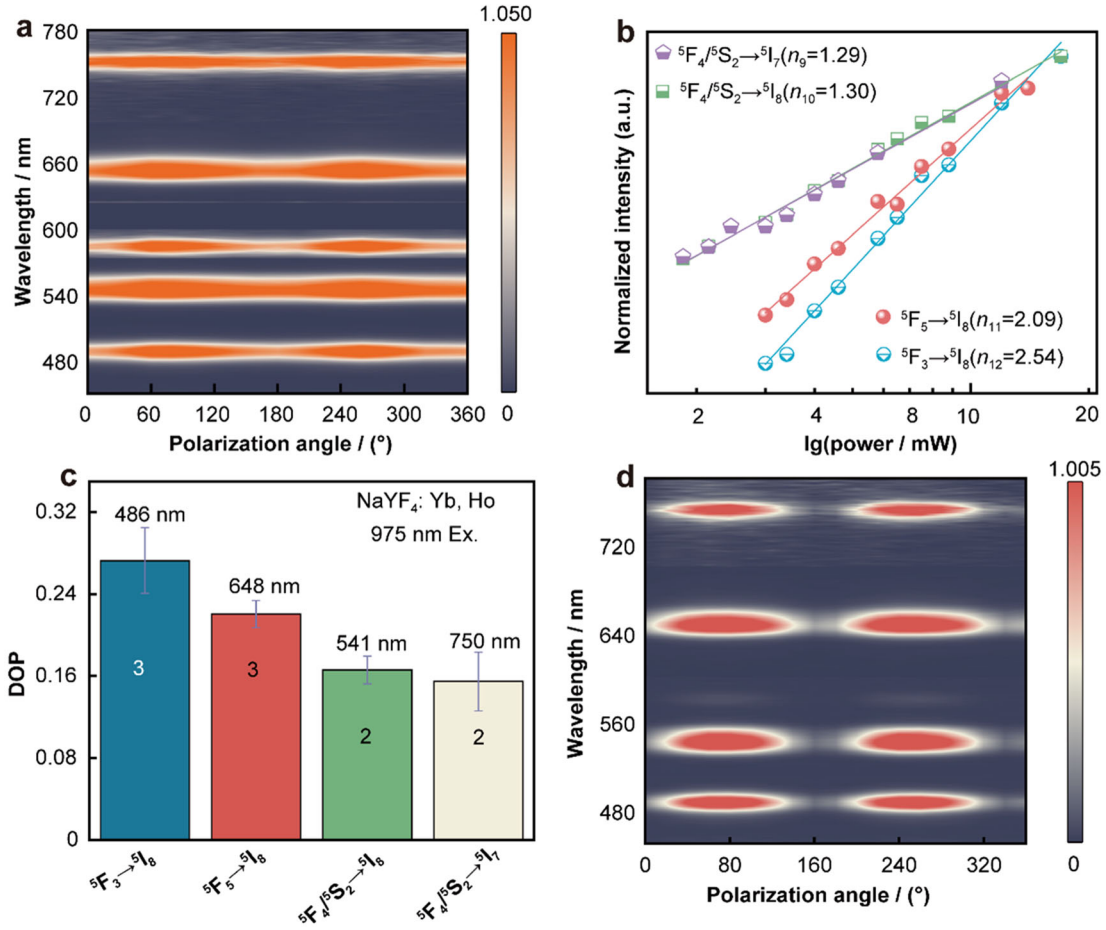

Fig. 4 Excitation wavelength regulating DOPs of PUCL synergistically: **a** matrix diagram of UCL spectra from $NaYF_4$: 20%Yb, 8%Ho single nanorod excited at 975 nm, where excitation power at 975 nm for all tests was 680 μW at ×100 objective, unless otherwise stated; **b** upconversion emission intensity as a function of excitation power for $NaYF_4$: 20%Yb, 8%Ho single nanorod excited by 975 nm; **c** histogram illustrating photon number connected DOPs of four transitions; **d** matrix diagram of UCL spectra from $NaYF_4$: 10%Gd, Ho single nanorod excited at 1150 nm

and 0.275, respectively (Fig. 5e). The second is the three-photon upconversion way (Fig. 5d); the DOPs of $^1G_4 \rightarrow {}^3H_6$ and $^1G_4 \rightarrow {}^3F_4$ transitions are 0.580 and 0.531, respectively (Fig. 5e). The third is the four-photon upconversion process (Fig. 5d); the DOP of $^1D_2 \rightarrow {}^3F_4$ transition is 0.925 (Fig. 5e). Evidently, the DOP for the four-photon process is larger than that for three-photon process. Furthermore, the DOPs from three-photon process are much greater than those from two-photon process. Those phenomena are highly coincident with the population density of ESs controlled by upconversion photons. In other words, the more the number of photons is required in upconversion process, the less the population density of ESs is (Fig. 5g). As a result, the fewer the mixing of different dipole orientations there exhibit, the larger the DOP of UCL it becomes. It is worth noting that a huge span of DOP from 0.925 to 0.233 is successfully achieved in Tm^{3+}, which is attributed to the large difference of population density in ESs based on four-photon and two-photon paths.

The modulation of DOPs from Tm^{3+} UCL can also be realized by adjusting the population density in ESs by power density of the excitation light. The population density in ESs of Tm^{3+} increases with growing pump power of the excitation light, leading to an obvious reduced trend of DOPs for all emissions (Fig. 5f). For the ES $^1D_2$ which originates from four-photon pump way (Fig. 5d, g), the population density rapidly increases with enhancing excitation power. Then, a mixture of irreducible transitions Γ_n ($^1D_2$) → Γ_m ($^3F_4$) with different dipole orientations is raised, resulting in a low proportion for similar dipole orientation and the small DOP of PUCL (Fig. 5g). This is analogous to the transitions of $^1G_4 \rightarrow {}^3H_6$, $^1G_4 \rightarrow {}^3F_4$, $^3F_3 \rightarrow {}^3H_6$ and $^3H_4 \rightarrow {}^3H_6$. Moreover, the reduced trend of DOP for the four-photon transition $^1D_2 \rightarrow {}^3F_4$ is more sensitive than that for the three-photon transitions $^1G_4 \rightarrow {}^3H_6$ and $^1G_4 \rightarrow {}^3F_4$, and three-photon transitions are faster than those for two-photon transition $^3H_4 \rightarrow {}^3H_6$. Therefore, the upconversion photons number regulated

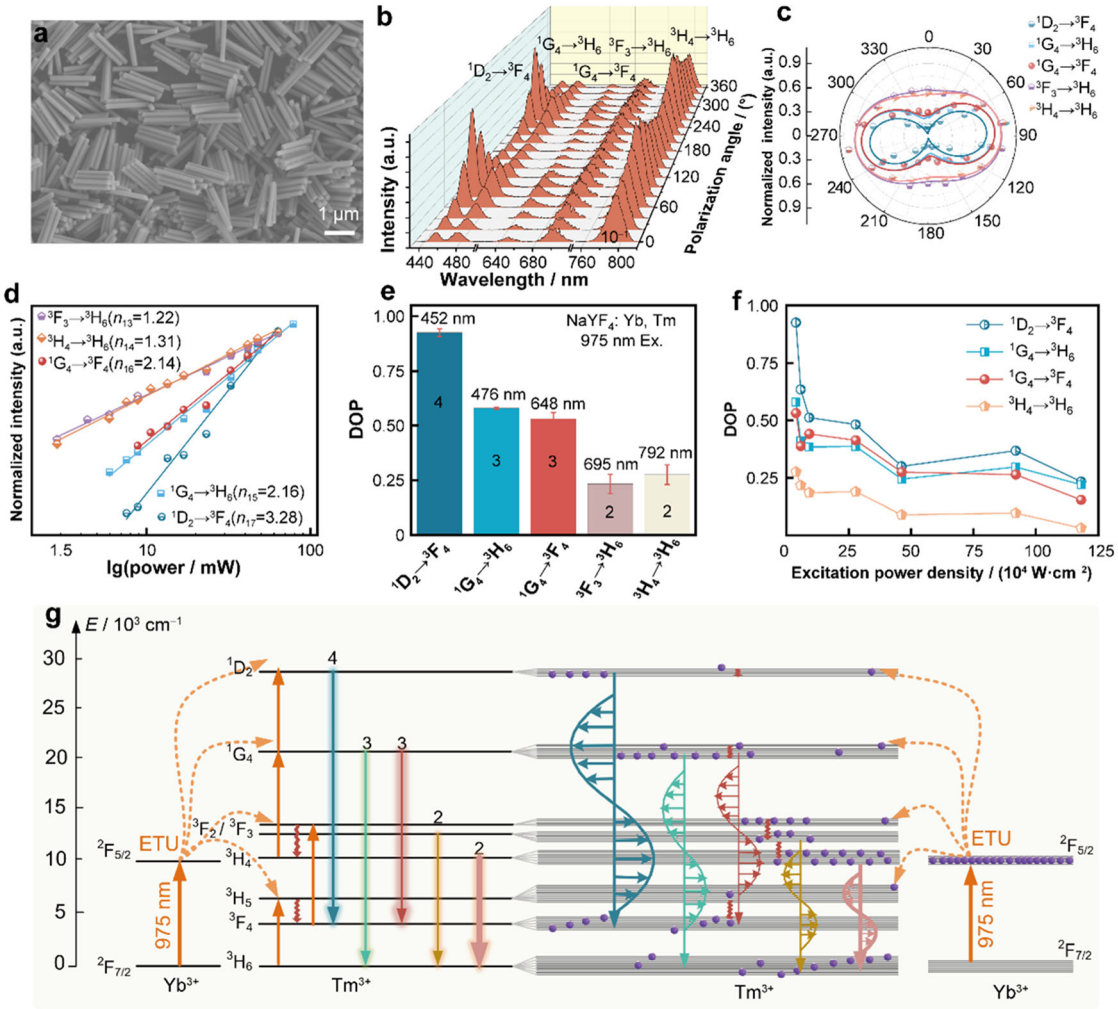

Fig. 5 Controlled DOPs from $NaYF_4$: Yb, Tm single nanorods based on number of upconversion photons: **a** SEM image of $NaYF_4$: 20%Yb, 5%Tm nanorods; **b** PUCL spectra from $NaYF_4$: Yb, Tm single nanorod excited at 975 nm, where excitation power at 975 nm for all tests was 680 μW at 100 × objective, unless otherwise stated; **c** polar plots of UCL integral intensities from $^1D_2 \rightarrow {}^3F_4$, $^1G_4 \rightarrow {}^3H_6$, $^1G_4 \rightarrow {}^3F_4$, $^3F_3 \rightarrow {}^3H_6$, $^3H_4 \rightarrow {}^3H_6$ transitions as a function of excitation polarization angle; **d** upconversion emission intensity as a function of excitation power for $NaYF_4$: 20%Yb, 5%Tm single nanorod excited by 975 nm; **e** histogram illustrating photon number connected DOPs of five transitions; **f** DOPs of different transitions as a function of excitation power density; **g** schematic diagram of energy transfer from Yb^{3+} to Tm^{3+}, accompanying with population density of ES_i and DOPs of different transitions

population density of ESs can be feedbacked by the DOPs from single nanorods and verified in Tm^{3+} and Ho^{3+}.

2.6 Multi-dimensional polarized anti-counterfeiting display and encryption

The PUCL of single nanorods is able to be applied in anti-counterfeiting displays with multi-dimensional encryption. Here, we introduce an encryption key by PUCL for anti-counterfeiting displays with full use of the low and high DOPs of $NaYF_4$: Yb, Ho nanorods upon excitation at 975 and 1150 nm, respectively. The low DOP excited by 975 nm can ensure the whole display of all the patterns, while the high DOP excited by 1150 nm is able to present the detail pictures, which provides an excellent opportunity for us to customize related patterns as polarized anti-counterfeiting displays. In detail, a rectangular groove is etched in silicon wafer as the pixel point for patterns by electron beam lithography (EBL) [51, 52] and reactive ion etching (RIE) (Fig. S7a). The width of the groove is less than the length of a single nanorod (Fig. S7b); thus, nanorods can only be filled into the grooves along rectangular groove (Fig. S7c, e). By software design, the rectangular groove can be arranged into any pattern with customizable size according to the designer's idea. Thus, we can consider the rectangular groove as a pixel point.

"G", "X" and "U" letters were first etched and filled by $NaYF_4$: Yb, Ho nanorods (Fig. 6a). The "G" and "U" are

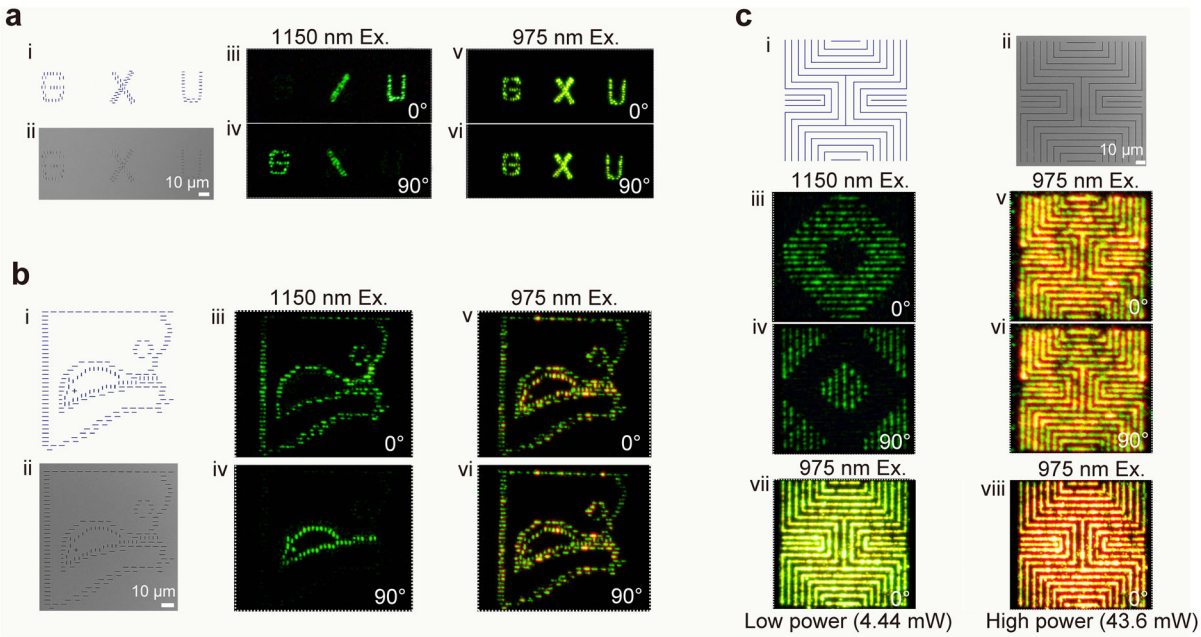

Fig. 6 Excitation polarized display and optical anti-counterfeiting with excitation power at 1150 nm of 93 mW at 10 × objective, and excitation power at 975 nm of 10.06 mW: **a** design (i) and SEM (ii) images of "G", "X" and "U" letters composed of $NaYF_4$: Yb, Ho nanorods, where pixels of "G" are arranged vertically, left slashes of "X" ("/") are arranged vertically, and right slashes ("\") are arranged horizontally, pixels of "U" are arranged horizontally (upconversion photoluminescence images of "G", "X" and "U" letters being excited by 1150 nm (iii–iv) or 975 nm (v–vi) with excitation polarized angle of 0° and 90°); **b** design (i) and SEM (ii) images of "Cat" and "Mouse" patterns composed of $NaYF_4$: Yb, Ho nanorods, where "Cat" is composed of horizontal pixel arrangement and "Mouse" is composed of vertical pixel arrangement (upconversion photoluminescence images of "Cat" and "Mouse" patterns being excited by 1150 nm (iii–iv) or 975 nm (v–vi) with excitation polarized angles at 0° and 90°); **c** design (i) and SEM (ii) images of "Labyrinth Totems" composed of $NaYF_4$: Yb, Ho nanorods, in which vertical nanowire grooves are arranged by vertical nanorods, and horizontal nanowire grooves are arranged by horizontal nanorods (upconversion photoluminescence images of "Labyrinth Totem" being excited by 1150 nm (iii–iv) or 975 nm (v–vi) with excitation polarized angle of 0° and 90°; upconversion photoluminescence images of "Labyrinth Totem" being excited by 975 nm with a low (vii) and high (viii) power, respectively)

arranged by vertical and horizontal nanorods, respectively. "X" is arrayed by vertical ("/") and horizontal ("\") nanorods, respectively (Fig. 6a-i, ii). Upon excitation at 1150 nm with a polarization angle of 0°, "U" and "/" of "X" letters are illuminated, while "\" of "X" and "G" letters are hidden (Fig. 6a-iii). When the angle was changed to 90°, "\" of "X" and "G" letters were displayed, while "U" and "/" of "X" letters disappeared (Fig. 6a-iv). At the same time, the whole letters "G", "X" and "U" can be completely shown under excitation at 975 nm due to the low DOP of nanorods (Fig. 6a-v, vi). Therefore, selective encryption and display can be realized by using different excitation wavelengths.

Graph encryption can be extended from the letter's encryption (Fig. 6b). The "Cat" and "Mouse" profiles are etched, where the "Cat" and "Mouse" are filled by horizontal and vertical nanorods, respectively (Fig. 6b-i, ii). We can see the "Cat" patterns when excitation is at 1150 nm and 0° of polarized angle (Fig. 6b-iii). While changing the polarized angle to 90°, the "Mouse" graph is presented (Fig. 6b-iv). In addition, when excited at 975 nm, the "Cat" and "Mouse" pictures are appeared simultaneously whenever the polarization angle of the excitation source (Fig. 6b-v, vi). These horizontal and vertical designs not only perform excellently in the encryption and hiding of words, but also present a brilliant performance in the anti-counterfeiting encryption of pictures.

Furthermore, high-polarized signal can be achieved in "Labyrinth Totem" composed of vertical and horizontal nanowire grooves (Fig. 6c-i, ii). The width of each nanowire groove is also smaller than the length of $NaYF_4$: Yb, Ho nanorods; thus, the nanorods can only be arrayed along the direction of nanowire grooves (Fig. S7d). Upon excitation at 1150 nm and 0° of polarized angle, a hollow diamond is presented (Fig. 6c-iii), which disappears when the excitation polarized angle is changed to 90° (Fig. 6c-iv). Moreover, the whole "Labyrinth Totem" is illuminated in orange color when excited by 975 nm (Fig. 6c-v, vi). Besides, the green (Fig. 6c-vii) and red (Fig. 6c-viii) colors of the whole "Labyrinth Totem" emerged when excitation at 975 nm with a low and high power, respectively. Finally, fivefold anti-counterfeiting is achieved. Our design provides multiple guarantees for anti-counterfeiting displays

and opens up infinite possibilities for polarized luminescence in designable patterns and multi-dimensional anti-counterfeiting displays.

3 Conclusion

In summary, we demonstrate a strategy to regulate the DOPs of PUCL from Ln^{3+}-doped single nanorods based on the number of upconversion photons. The core of this strategy is the population density of ESs tuned by the number of upconversion photons. Compared with the two-photon ESs, population density of ESs, which required much more photons, is lower. The lower population density generates a higher possibility of similar dipole orientation and a larger DOP of PUCL. The modulation of the DOPs of PUCL from Ho^{3+} and Tm^{3+} is realized by cross-relaxation, excitation wavelength, excitation power density, and changes in local site symmetry. The DOPs have been controlled from 0.233 of the two-photon upconversion process to 0.925 of the four-photon upconversion process in Tm^{3+}. Besides, taking advantage of the highly polarized nature of single nanorods, multi-dimensional anti-counterfeiting display and encryption in words, pictures, and labyrinth totem have been realized. This regulated polarization strategy will promote the development of PUCL from Ln^{3+}-doped nanoparticles. The tunable polarization properties combined with multi-dimensional encryption methods enable potential applications in three-dimensional display, optical encoding, and many other emerging fields.

Acknowledgements This study was financially supported by the National Natural Science Foundation of China (Nos. 11704081, 52125205, 52250398, U20A20166, 52192614 and 52003101), Guangxi Natural Science Foundation (Nos. 2020GXNSFAA297182, 2020GXNSFAA297041 and 2017GXNSFBA19-8229), the special fund for "Guangxi Bagui Scholars," National Science and Technology Innovation Talent Cultivation Program (No. 2023BZRC016) National Key R&D Program of China (Nos. 2021YFB3200302 and 2021YFB3200304), the Natural Science Foundation of Beijing Municipality (No. 2222088), Shenzhen Science and Technology Innovation Program (No. KQTD20170810105439418) and the Fundamental Research Funds for the Central Universities.

Declarations

Conflict of interests Cao-Feng Pan is an Editorial Board Member for *Rare Metals* and was not involved in the editorial review or the decision to publish this article. All authors declare that there are no competing interests.

References

[1] Zhou J, Chen G, Wu E, Bi G, Wu B, Teng Y, Zhou S, Qiu J. Ultrasensitive polarized up-conversion of Tm^{3+}–Yb^{3+} doped β-$NaYF_4$ single nanorod. Nano Lett. 2013;13(5):2241. https://doi.org/10.1021/nl400807m.

[2] Binnemans K. Interpretation of europium(III) spectra. Coord Chem Rev. 2015;295:1. https://doi.org/10.1016/j.ccr.2015.02.015.

[3] Wei S, Shang X, Huang P, Zheng W, Ma E, Xu J, Zhang M, Tu D, Chen X. Polarized upconversion luminescence from a single $LiLuF_4$:Yb^{3+}/Er^{3+} microcrystal for orientation tracking. Sci China Mater. 2022;65:220. https://doi.org/10.1007/s40843-021-1713-x.

[4] Zhou B, Shi B, Jin D, Liu X. Controlling upconversion nanocrystals for emerging applications. Nat Nanotechnol. 2015;10:924. https://doi.org/10.1038/nnano.2015.251.

[5] Jiang YF, Guo CY, Zhang XF, Cheng XL, Huo LH, Wang TT, Xu YM. Er_2O_3 nanospheres with fast response to humidity for non-contact sensing. Rare Met. 2023;42(1):56. https://doi.org/10.1007/s12598-022-02165-0.

[6] Chen HJ, Luo X, Wang XD, Mao HM, Zeng XH, Xu K. Structural and luminescent properties of GaN:Eu. Dy films. Chin J Rare Met. 2023;47(324):381. https://doi.org/10.13373/j.cnki.cjrm.XY22060011.

[7] Guo Y, Qin LJ, Xu J, Jiang XP, Yue XY, Hou Y, Shi H, Wang LX, Zhang QT. Stark splitting of intense red emission for Er^{3+} in Oh symmetry sites realizing optical temperature sensing in biological applications. Rare Met. 2024;43(3):1263. https://doi.org/10.1007/s12598-023-02520-9.

[8] Zhuang Y, Chen D, Chen W, Zhang W, Su X, Deng R, An Z, Chen H, Xie RJ. X-ray-charged bright persistent luminescence in $NaYF_4$:Ln^{3+}@$NaYF_4$ nanoparticles for multidimensional optical information storage. Light Sci Appl. 2021;10:132. https://doi.org/10.1038/s41377-021-00575-w.

[9] Pu R, Zhan Q, Peng X, Liu S, Guo X, Liang L, Qin X, Zhao ZW, Liu X. Super-resolution microscopy enabled by high-efficiency surface-migration emission depletion. Nat Commun. 2022;13:6636. https://doi.org/10.1038/s41467-022-33726-7.

[10] Panov N, Lu D, Ortiz-Rivero E, Rodrigues EM, Haro-González P, Jaque D, Hemmer E. Hyperspectral imaging and optical trapping: complementary tools for assessing direction-dependent polarized emission from single upconverting $LiYF_4$:Yb^{3+}/Er^{3+} microparticles. Adv Opt Mater. 2021;9(12):2100101. https://doi.org/10.1002/adom.202100101.

[11] Huang H, Wang S, Chen R, Zhang N, Yao HR, Zheng Y, Huang F, Chen D. Engineering upconverting core-shell nano-probe for spectral responsive fluid velocimetry. Nano Res. 2023;16:1212. https://doi.org/10.1007/s12274-022-4636-4.

[12] Huang H, Huang F, Lin L, Feng Z, Cheng Y, Wang Y, Chen D. Perceiving linear-velocity by multiphoton upconversion. ACS Appl Mater Inter. 2019;11(49):46379. https://doi.org/10.1021/acsami.9b17507.

[13] Zhao JB, Wu LL. Yb^{3+}- and Er^{3+}-doped Y_2O_3 microcrystals for upconversion photoluminescence and energy transfer with enhancements of near-ultraviolet emission. Rare Met. 2021;40(2):123. https://doi.org/10.1007/s12598-019-01269-4.

[14] Wang LM, Liu WY, Hu ML, Yao JS, Wang P, Liu JH, He M, Gao Y, Li ZX. Rare earth-based MOF@mesoporous silica nanoplatform for long-term and luminescence trackable chemotherapy. Rare Met. 2022;41(8):2701. https://doi.org/10.1007/s12598-022-01978-3.

[15] Li YL, Li NN, Wang D, Chu F, Lee SD, Zheng YW, Wang QH. Tunable liquid crystal grating based holographic 3D display system with wide viewing angle and large size. Light Sci Appl. 2022;11:188. https://doi.org/10.1038/s41377-022-00880-y.

[16] Zheng NN, Kong WY, Huang Z, Liu XJ, Liang SH, Deng GY, Zhao LJ, Lu J. Novel theranostic nanoagent based on $CuMo_2S_3$-PEG-Gd for MRI-guided photothermal/

photodynamic/chemodynamic therapy. Rare Met. 2022;41(1):45. https://doi.org/10.1007/s12598-021-01793-2.
[17] Ding Y, Yuan Z, Hu JW, Xu K, Wang H, Liu P, Cai KY. Surface modification of titanium implants with micro–nano-topography and NIR photothermal property for treating bacterial infection and promoting osseointegration. Rare Met. 2022;41(2):673. https://doi.org/10.1007/s12598-021-01830-0.
[18] Zhou H, Zeng X, Li A, Zhou W, Tang L, Hu W, Fan Q, Meng X, Deng H, Duan L, Li Y, Deng Z, Hong X, Xiao Y. Upconversion NIR-II fluorophores for mitochondria-targeted cancer imaging and photothermal therapy. Nat Commun. 2020;11:6183. https://doi.org/10.1038/s41467-020-19945-w.
[19] Zhanghao K, Chen X, Liu W, Li M, Liu Y, Wang Y, Luo S, Wang X, Shan C, Xie H, Gao J, Chen X, Jin D, Li X, Zhang Y, Dai Q, Xi P. Super-resolution imaging of fluorescent dipoles via polarized structured illumination microscopy. Nat Commun. 2019;10:4694. https://doi.org/10.1038/s41467-019-12681-w.
[20] Kim J, Michelin S, Hilbers M, Martinelli L, Chaudan E, Amselem G, Fradet E, Boilot JP, Brouwer AM, Baroud CN, Peretti J, Gacoin T. Monitoring the orientation of rare-earth-doped nanorods for flow shear tomography. Nat Nanotechnol. 2017;12:914. https://doi.org/10.1038/nnano.2017.111.
[21] Kim J, Chacón R, Wang Z, Larquet E, Lahlil K, Leray A, Colas-des-Francs G, Kim J, Gacoin T. Measuring 3D orientation of nanocrystals via polarized luminescence of rare-earth dopants. Nat Commun. 2021;12:1943. https://doi.org/10.1038/s41467-021-22158-4.
[22] Du K, Feng J, Gao X, Zhang H. Nanocomposites based on lanthanide-doped upconversion nanoparticles: diverse designs and applications. Light Sci Appl. 2022;11:222. https://doi.org/10.1038/s41377-022-00871-z.
[23] Liu, X, Lin, ZX, Shi, YB, Wang XY, Ding MY, Yang XF. Dynamic manipulation of multimodal emission in Er^{3+}-activated non-core-shell structure for optical thermometry and information security. Rare Met. 2024;43(4):1702. https://doi.org/10.1007/s12598-023-02492-w.
[24] Huang H, Chen J, Liu Y, Lin J, Wang S, Huang F, Chen D. Lanthanide-doped core@multishell nanoarchitectures: multimodal excitable upconverting/downshifting luminescence and high-level anti-counterfeiting. Small. 2020;16(19):2000708. https://doi.org/10.1002/smll.202000708.
[25] Lai X, Ren Q, Vogelbacher F, Sha WEI, Hou X, Yao X, Song Y, Li M. Bioinspired quasi-3D multiplexed anti-counterfeit imaging via self-assembled and nanoimprinted photonic architectures. Adv Mater. 2022;34(3):2107243. https://doi.org/10.1002/adma.202107243.
[26] Yao W, Tian Q, Wu W. Tunable emissions of upconversion fluorescence for security applications. Adv Opt Mater. 2019;7(6):1801171. https://doi.org/10.1002/adom.201801171.
[27] Li P, Li F, Zhang X, Li Y, Luo X, Wang R, Cai Y, Zhang Y. Orthogonally polarized luminescence of single bismuth phosphate microcrystal doped with europium. Adv Opt Mater. 2020;8(17):2000583. https://doi.org/10.1002/adom.202000583.
[28] Xie Y, Song Y, Sun G, Hu P, Bednarkiewicz A, Sun L. Lanthanide-doped heterostructured nanocomposites toward advanced optical anti-counterfeiting and information storage. Light Sci Appl. 2022;11:150. https://doi.org/10.1038/s41377-022-00813-9.
[29] Zhou X, Ning L, Qiao J, Zhao Y, Xiong P, Xia Z. Interplay of defect levels and rare earth emission centers in multimode luminescent phosphors. Nat Commun. 2022;13:7589. https://doi.org/10.1038/s41467-022-35366-3.
[30] Chen X, Liu Y, Tu D. Optical spectroscopy of lanthanide-doped nanoparticles. Nanomed Nanotoxicol. 2014. https://doi.org/10.1007/978-3-642-40364-4_5.
[31] Liu MM, Zheng GC, Wei Y, Tian D, Zheng QB, Huang L, Xie J. Doping induced morphology, crystal structure, and upconversion luminescence evolution: from Na_3ScF_6:Yb/Er/Y to $NaYF_4$:Yb/Er/Sc nanocrystals. Rare Met. 2023;42(3):1018. https://doi.org/10.1007/s12598-022-02159-y.
[32] Yang D, Peng Z, Guo X, Qiao S, Zhao P, Zhan Q, Qiu J, Yang Z, Dong G. Tunable light polarization information from single upconverting fluoride microcrystal. Adv Opt Mater. 2021;9(13):2100044. https://doi.org/10.1002/adom.202100044.
[33] Yang D, Peng Z, Zhan Q, Huang X, Peng X, Guo X, Dong G, Qiu J. Anisotropic excitation polarization response from a single white light-emitting β-$NaYF_4$:Yb^{3+}, Pr^{3+} microcrystal. Small. 2019;15(43):1904298. https://doi.org/10.1002/smll.201904298.
[34] Chen P, Song M, Wu E, Wu B, Zhou J, Zeng H, Liu X, Qiu J. Polarization modulated upconversion luminescence: single particle vs. few-particle aggregates. Nanoscale. 2015;7(15):6462. https://doi.org/10.1039/c5nr00289c.
[35] Lyu ZY, Dong H, Yang XF, Sun LD, Yan CH. Highly polarized upconversion emissions from lanthanide-doped $LiYF_4$ crystals as spatial orientation indicators. J Phys Chem Lett. 2021;12(46):11288. https://doi.org/10.1021/acs.jpclett.1c03409.
[36] Chen L, Rong Y, Ren M, Wu W, Qin M, Pan C, Ma Q, Liu S, Wu B, Wu E, Xu J, Zeng H. Selective polarization modification of upconversion luminescence of $NaYF_4$:Yb^{3+}, Er^{3+} nanoparticles by plasmonic nanoantenna arrays. J Phys Chem C. 2018;122(27):15666. https://doi.org/10.1021/acs.jpcc.8b03975.
[37] He J, Zheng W, Ligmajer F, Chan CF, Bao Z, Wong KL, Chen X, Hao J, Dai J, Yu SF, Lei DY. Plasmonic enhancement and polarization dependence of nonlinear upconversion emissions from single gold nanorod@SiO_2@CaF_2:Yb^{3+}, Er^{3+} hybrid core–shell–satellite nanostructures. Light Sci Appl. 2017;6:e16217. https://doi.org/10.1038/lsa.2016.217.
[38] Tu D, Liu Y, Zhu H, Li R, Liu L, Chen X. Breakdown of crystallographic site symmetry in lanthanide-doped $NaYF_4$ crystals. Angew Chem. 2013;125(4):1166. https://doi.org/10.1002/ange.201208218.
[39] Gruber JB, Hills ME, MacFarlane RM, Morrison CA, Turner GA. Symmetry, selection rules, and energy levels of Pr^{3+}:$Y_3Al_5O_{12}$. Chem Phys. 1989;134(2–3):241. https://doi.org/10.1016/0301-0104(89)87159-9.
[40] Kolesov R, Xia K, Reuter R, Stöhr R, Zappe A, Meijer J, Hemmer PR, Wrachtrup J. Optical detection of a single rare-earth ion in a crystal. Nat Commun. 2012;3:1029. https://doi.org/10.1038/ncomms2034.
[41] Zhou J, Chen G, Zhu Y, Huo L, Mao W, Zou D, Sun X, Wu E, Zeng H, Zhang J, Zhang L, Qiu J, Xu S. Intense multiphoton upconversion of Yb^{3+}–Tm^{3+} doped β-$NaYF_4$ individual nanocrystals by saturation excitation. J Mater Chem C. 2015;3(2):364. https://doi.org/10.1039/C4TC02363C.
[42] Kuang Y, Xu J, Wang C, Li T, Gai S, He F, Yang P, Lin J. Fine-tuning Ho-based red-upconversion luminescence by altering $NaHoF_4$ core size and $NaYbF_4$ shell thickness. Chem Mater. 2019;31(19):7898. https://doi.org/10.1021/acs.chemmater.9b01944.
[43] Huang X, Han S, Huang W, Liu X. Enhancing solar cell efficiency: the search for luminescent materials as spectral converters. Chem Soc Rev. 2013;42(1):173. https://doi.org/10.1039/c2cs35288e.
[44] Pollnau M, Gamelin DR, Lüthi SR, Güdel HU, Hehlen MP. Power dependence of upconversion luminescence in lanthanide and transition-metal-ion systems. Phys Rev B. 2000;61(5):3337. https://doi.org/10.1103/physrevb.61.3337.
[45] Liu H, Huang K, Valiev RR, Zhan Q, Zhang Y, Ågren H. Photon upconversion kinetic nanosystems and their optical response. Laser Photon Rev. 2018;12(1):1700144. https://doi.org/10.1002/lpor.201700144.

[46] Suyver JF, Aebischer A, García-Revilla S, Gerner P, Güdel HU. Anomalous power dependence of sensitized upconversion luminescence. Phys Rev B. 2005;71(12):125123. https://doi.org/10.1103/physrevb.71.125123.
[47] Martín-Rodríguez R, Meijerink A. Infrared to near-infrared and visible upconversion mechanisms in $LiYF_4$: Yb^{3+}, Ho^{3+}. J Lumin. 2014;147:147. https://doi.org/10.1016/j.jlumin.2013.11.008.
[48] Villanueva-Delgado P, Krämer KW, Valiente R. Simulating energy transfer and upconversion in β-$NaYF_4$: Yb^{3+}, Tm^{3+}. J Phys Chem C. 2015;119(41):23648. https://doi.org/10.1021/acs.jpcc.5b06770.
[49] Zuo SL, Chen P, Pan CF. Mechanism of magnetic field-modulated luminescence from lanthanide ions in inorganic crystal: a review. Rare Met. 2020;39(10):1113. https://doi.org/10.1007/s12598-020-01450-0.
[50] Wang F, Han Y, Lim CS, Lu Y, Wang J, Xu J, Chen H, Zhang C, Hong M, Liu X. Simultaneous phase and size control of upconversion nanocrystals through lanthanide doping. Nature. 2010;463:1061. https://doi.org/10.1038/nature08777.
[51] Chen P, Pan J, Gao W, Wan B, Kong X, Cheng Y, Liu K, Du S, Ji W, Pan C, Wang ZL. Anisotropic carrier mobility from 2H WSe_2. Adv Mater. 2022;34(7):2108615. https://doi.org/10.1002/adma.202108615.
[52] Zhang Q, Zuo S, Chen P, Pan C. Piezotronics in two-dimensional materials. InfoMat. 2021;3(9):987. https://doi.org/10.1002/inf2.12220.